ENGINE INSTALLATION AND SOUND PROPAGATION EFFECTS ON AIRCRAFT NOISE LEVELS IN NOISE CONTROL POINTS

O.I.Zaporozhets[a], V.I.Tokarev[b], G.G.Golembievskiy

National Aviation University, NAU,
Avenue Cosmonaut Komarov 1, 03058 Kyiv, Ukraine

[a]zap@nau.edu.ua, [b]vadim_tok@SoftHome.net

Calculation method for assessment of the atmosphere influence on sound propagation and engine installation effects are considered. The algorithm of sound ray path is analyzed in presence of shielding and reflecting surfaces which are character for current and perspective aircraft types, so as for wind velocity and temperature gradients for sound refraction parameters of the atmosphere.

Introduction

Aircraft noise levels are defined by sound propagation and engine installation effects sufficiently. Their correct taking in consideration may improve the noise calculation greatly. For that particular models were investigated.

Sound propagation models include the following effects: geometrical divergence, atmospheric absorption, ground effect (reflection from surface covering), meteorological effects (refraction in air).

Installation effects of the engines are considered of four types: sound shielding by wing; sound shielding by fuselage; sound reflection by wing; sound refraction by jets.

1. Review of sound spreading

This refers to the spreading of sound energy as a result of the expansion of the wave front. Geometric spreading is independent of frequency and has a major effect in almost all sound propagation situations. There are two common kinds of geometric spreading: spherical and cylindrical spreading.

In the case of spherical spreading from a point source or at distances from a large source, which are much larger than characteristic source dimensions, in a loss-less medium with no reflections the sound intensity is related to power and range by (Fig. 1):

$$I = p^2(r)/\rho c = W/4\pi r^2 \qquad (1)$$

where: I = acoustic intensity (watts/m^2), $p(r)$ = sound pressure at radial distance r (N/m^2), r = distance from the source in meters, W = sound power (watts), ρc = acoustic impedance (rayls).

In terms of sound levels this translates to:

$$SPL = SWL - 20 \log r - 10 \log [W_{ref} \rho c / (p^2_{ref} 4\pi)] \qquad (2)$$

where: SWL - sound power level (dB re 10^{-12} Watts), SPL - sound pressure level (dB re $2\text{x}10^{-5}$ N/m^2).

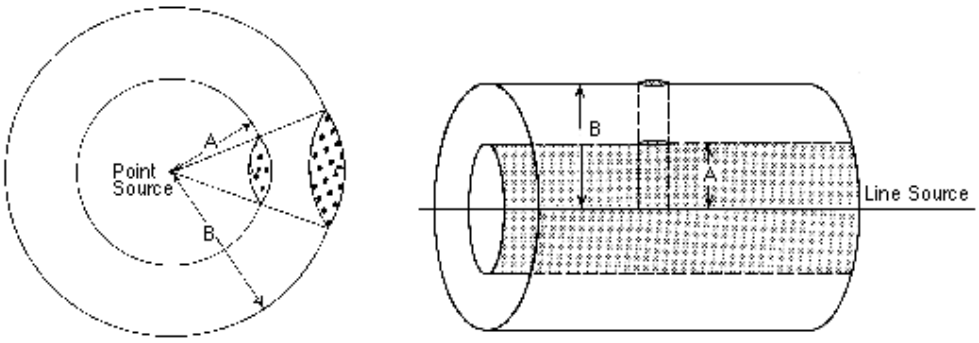

Figure 1 – Sound wave spreading from point and line sources

A line source will produce cylindrical spreading, resulting in a sound level reduction of 3 dB per doubling of distance, so the intensity decreases directly according to the distance from the source. Radii A and B in Fig. 1 indicate a doubling of distance. The moving aircraft is represented as an axially-symmetric noise source, around which the cylindrical surfaces with constant noise levels are formed. The central axis of these cylinders is coincident with the flight path axis and the radius of particular cylinder surface is defined as the noise radius for a given noise level [1].

The power of the dependence of the time-integrated sound level (noise impact indeces like *EPNL*, *SEL*, etc.) on the distance tends to 1 for a moving source, not to 2, as it would for point source and instantaneous sound levels like *OASPL, $L_A(f)$, PNL(t)*. It should be noted however that atmospheric absorption was neglected and in real conditions the exponent would be somewhat higher.

Usually the source is directional, thus an additional term - Directivity Index *DI*, (correction ΔL_Θ for directivity of sound radiation in some known methods, for example [2]) is needed to account for the uneven distribution of the sound intensity as a function of direction. The directivity index is the difference between the actual sound pressure and the sound pressure from a non-directional point source with the same total acoustic power. It can be determined experimentally or calculated for a limited number of analytical cases, such as classical cases - a piston in a baffle (a decent approximation of a loudspeaker), a piston in the end of a long tube, or classical aircraft noise case – noise radiation by jets:

$$DI = 10\log_{10} Q; \qquad (3)$$

where directivity factor $Q = I_\theta / I_{mean} = p_\theta^2 / p_s^2$; pP_θ – *rms* sound pressure at angle θ for the directional source, p_s – *rms* sound pressure of non-directional point source radiating the same total power.

For an omni-directional source radiating into free space *DI* = 0 dB. General purpose propagation equation without reflection is then:

$$SPL = SWL - 20\log r - 11 + DI. \qquad (4)$$

Directivity index is necessary first of all for taxiing or rolling aircraft and for engine testing noise calculations. If a specific directivity pattern is not available the generalized directivity patterns according to the type of the engine may be proposed, Fig. 2. Distinctions between specific directivity patterns and the generalized relationship proposed by ICAO [2] may be as large as 10 dB(A) in certain directions.

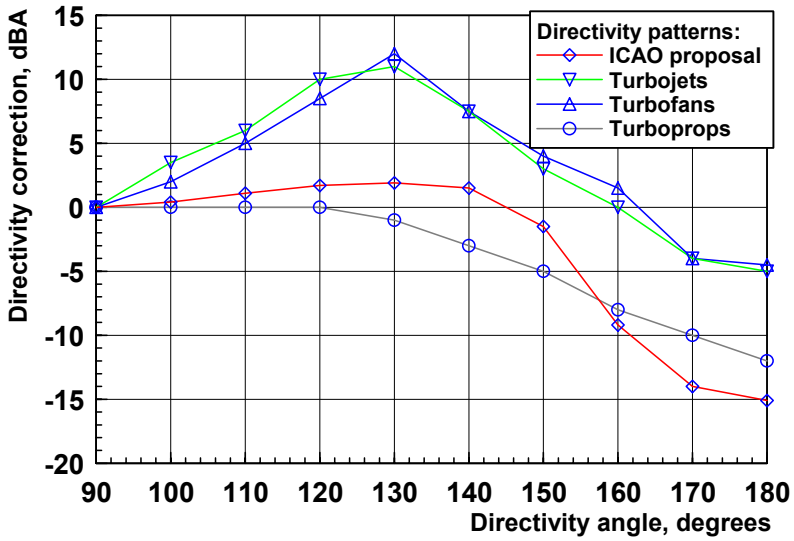

Figure 2 – Generalized directivity patterns for characteristic engine types

2. Absorption of sound in the air

Air absorption is an important factor in free-field sound propagation. A very comprehensive work has been carried out before issuing ISO 9613-1 [5]. It is recommended to follow the calculation procedure laid down in [5] as also recommended in IEC 1094-3 [19].

For a standard pressure of 1 atm the absorption coefficient α (in dB/100m) can be calculated as a function of frequency f (Hz), temperature T (degrees Kelvin) and molar concentration of water vapor h (%) by:

$$\alpha = 869 \times f^2 \left\{ 1.84 \times 10^{-11} \left(\frac{T}{T_0}\right)^{1/2} + \left(\frac{T}{T_0}\right)^{-5/2} \left[0.01275 \frac{e^{-2239.1/T}}{F_{r,O} + f^2 / F_{r,O}} + 0.1068 \frac{e^{-3352/T}}{F_{r,N} + f^2 / F_{r,N}} \right] \right\},$$

$$F_{r,O} = 24 + 4.04 \times 10^4 h \frac{0.02 + h}{0.391 + h}, \qquad (5)$$

$$F_{r,N} = \left(\frac{T}{T_0}\right)^{-1/2} \left(9 + 280 h e^{\left\{ -4.17 \left[\left(\frac{T}{T_0}\right)^{-1/3} - 1 \right] \right\}} \right).$$

The actual attenuation due to atmospheric absorption A_{abs} (dB) for a given propagation range can be expressed by:

$$A_{abs} = \alpha r / 100 \quad \text{(dB)},$$

where r is traveling distance.

The methods of absorption coefficient calculation were compared for FAR 36 [22] and outlined above algorithm based on ISO standards with Sutherland [21] data. The numerical results for absorption coefficient for ambient temperature 0^0, 10^0, 20^0, 30^0C and relative humidity 10, 20, 30, 50, 70, 90% were calculated and compared. The strict comparison of the models with Sutherland results for temperatures 0 and 20 ^{0}C are shown in fig. 3. As follows from the cases the attenuation below frequency 500 Hz is very low unless distance of sound propagation would be great. Best results are shown by algorithm of ISO method that is recommended for implementation in aircraft noise calculations.

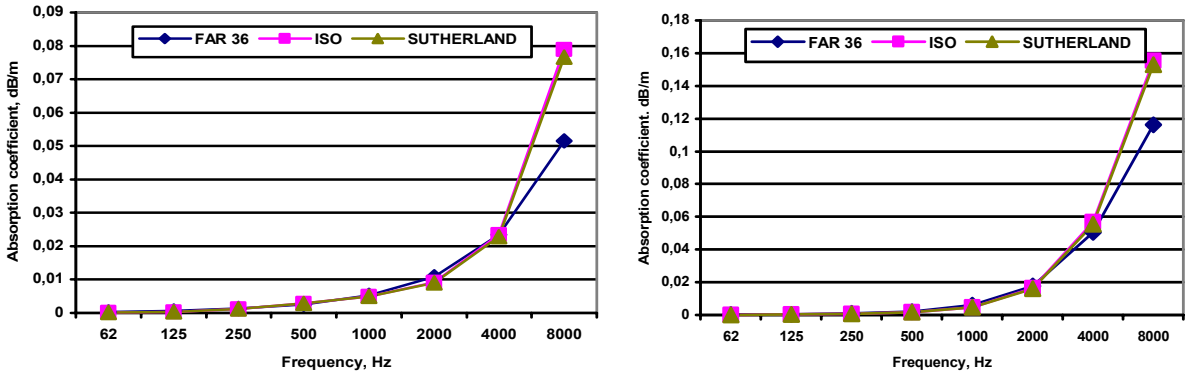

Figure 3 - comparison of the calculated results with Sutherland measurement for temperatures 20 (a) and 0 ^{0}C (b)

It must be concluded that ISO 9613-1 and FAR 36 (CFR PART 36, section A36.7.2 of 14) models can be used for the purposes of atmospheric absorption. Both models are very similar between one another at the whole range of atmosphere conditions, possible in operation, specially at middle and high frequencies. At low frequencies the results for the model ISO are much less than for model FAR 36. Advantage of the model ISO – a strict physical phenomena in its foundation. Advantage of the model FAR 36– it is more simple in calculation.

3. Sound propagation near to homogeneous impedance ground surfaces

Aircraft noise calculation method must include an assessment of sound propagation over the reflecting ground surface with homogeneous impedance characteristics. The exact solution of the problem was given in [8 - 20] for various conditions (different impedance of the ground and the geometrical scheme of the sound event) and types (monopole, dipole, quadrupole) of acoustic sources. Strict mathematical formulation of the problem is given in [21]. The effect was investigated and presented for aircraft flight modes in [22] and ground operation modes in [23].

Sound reflection model shall be ready for use only with accurate input data for the ground impedance, which is an important parameter. Soft surfaces have a relatively low impedance, which leads to a high ground attenuation, and thus to lower sound pressure levels at receiver point. The ground behaviour is strongly dependent on frequency.

The purpose of an impedance model is to describe how the impedance varies with frequency, and possibly how it depends on other physical parameters of the ground covering, such as its porosity, flow resistivity, etc. Most popular among them is an one-parameter model of impedance [24]:

$$Z_{ni} = 1 + 9{,}08\left(\frac{1000f}{\sigma}\right)^{-0{,}75} + i11{,}9\left(\frac{1000f}{\sigma}\right)^{-0{,}75}. \qquad (6)$$

As a rough guideline, σ in (6) should be between 20 000 (soft snow) and 20 000 000 (old asphalt). It has the same unit (Ns/m^4) as the flow resistivity. This model is developed to be good for high frequencies and is not necessarily suitable for low frequencies.

If there is a relatively soft layer on top of a hard surface, such as snow on frozen ground, the following modified one-parameter model shall be used:

$$\begin{aligned} Z_n &= Z_{ni} i \cot(Lk); \\ k &= \frac{2\pi f}{c}\left[1 + 10{,}8\left(\frac{1000f}{\sigma}\right)^{-0{,}7} + i10{,}3\left(\frac{1000f}{\sigma}\right)^{-0{,}59}\right], \end{aligned} \qquad (7)$$

where Z_{ni} is the impedance obtained from equation (7), and L is the best estimate of the porous layer depth.

In some situations, like snow covered ground, the one-parameter model may not yield any good results. Then an alternative approach is to use a two parameter model. If one of the parameters can be measured, like the layer depth in the model below, the same principle can be used as for the one parameter model.

If the flow resistivity is rather high and the porosity changes with depth, the following model gives a better description [24]:

$$Z = 0{,}484(1+i)\sqrt{\frac{\sigma_e}{f}} + 30i\frac{\alpha_e}{f}, \qquad (8)$$

where flow resistivity σ_e is not the same parameter as in the previously presented models.

In [25] there is also a 4-parameter model given by

$$\begin{aligned} Z &= \frac{\rho_b(\varpi)}{k_b \rho}; \\ k_b^2(\omega) &= \gamma\Omega\left[\left(\frac{4}{3} - \frac{\gamma - 1}{\gamma} N_{pr}\right)\frac{q^2}{\Omega} + \frac{i4s_p^2\sigma}{\omega\rho}\right]; \\ \rho_b(\omega) &= \rho\left(\frac{4q^2}{3\Omega} + i\frac{4s_p^2}{\omega\rho}\right). \end{aligned} \qquad (9)$$

In the above equations σ is the flow resistivity, Ω is the volume porosity, T is the tortuosity, s_p is the pore shape factor, ρ is the air density, γ is the ratio of specific heats and N_{pr} is the Prandtl number. This model is best suitable for low frequencies and/or large σ.The accuracy of acoustical impedance models has been established by comparison with measurements of surface characteristics. Some results of comparison are shown in Fig. 4, 5. Following models are used in the analysis: AT4 –

4-parameters model (9), AT – 2-parameters model (8), BD - model (6). Measurements were made in Open University (OU) and Silsoe (Sil) [26].

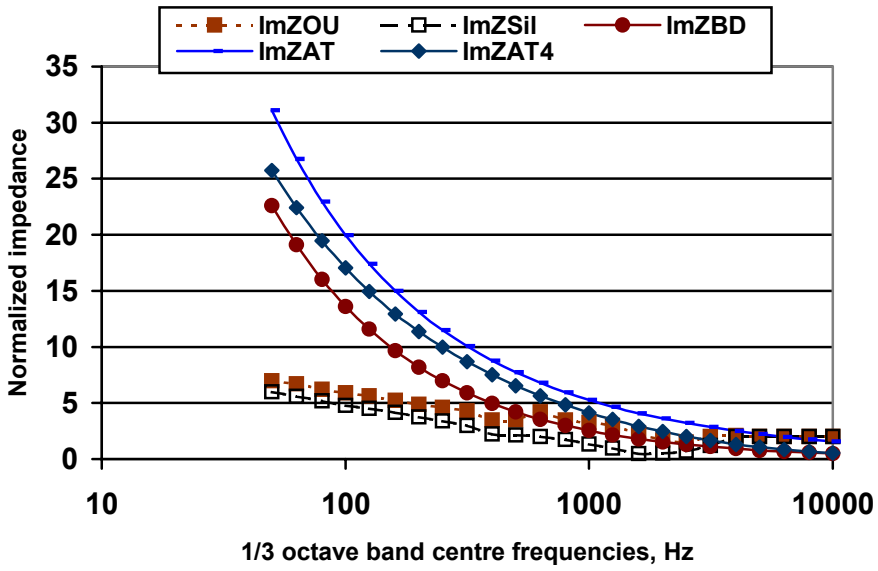

Figure 4 – Measured (Open University, ZOU, and Silsoe, ZSil) and calculated imaginary parts of impedance for grass covering

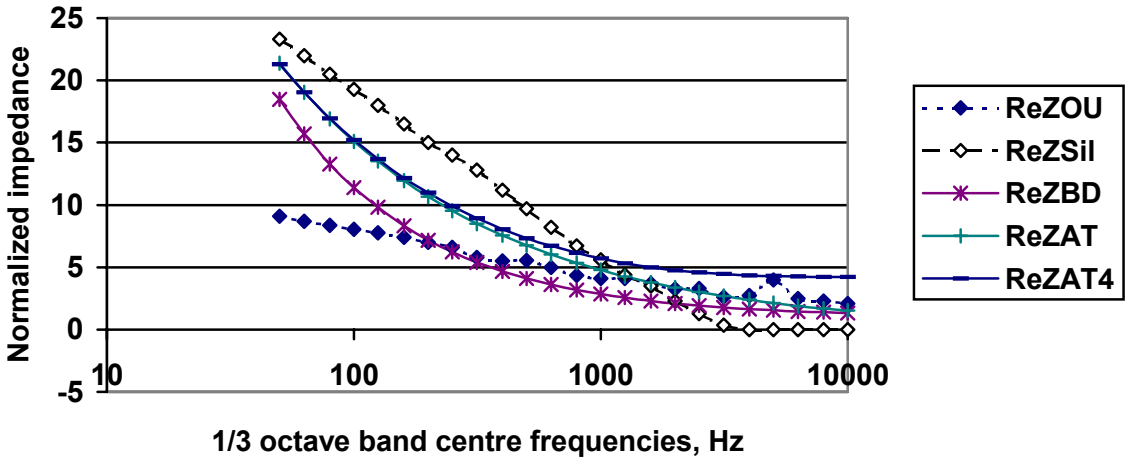

Figure 5 – Measured (Open University, ZOU, and Silsoe, ZSil) and calculated real parts of impedance for grass covering

The 4-parameters (9) and 2-parameters (8) models are more strict in their physical phenomena description, but their accuracy for most possible cases is the same as for 1-parameter model (6).

In Fig. 6 (Fig. 5.14 in [27]) the measured values are compared to those obtained using the one-parameter model and $\sigma = 150000$. Note that in the theoretical values the real part becomes larger than the imaginary one for frequencies higher than 630 Hz, but in the measured case the imaginary part is always larger.

For frequencies lower than 250 Hz a good result cannot be gotten. This is due to the fact that the impedance is very high at these frequencies, but also to the fact that the method requires much higher receiver positions to capture the minimum in this

case. This showed up as impedance values at the edge of the searched domain and/or large errors. For frequencies higher that 1000 Hz, the method gave the minimum error at the edge of the searched domain and also high errors, probably caused by insufficient microphone spacing and meteorological disturbances [27]. The same result is obtained in our calculations (see Fig. 6).

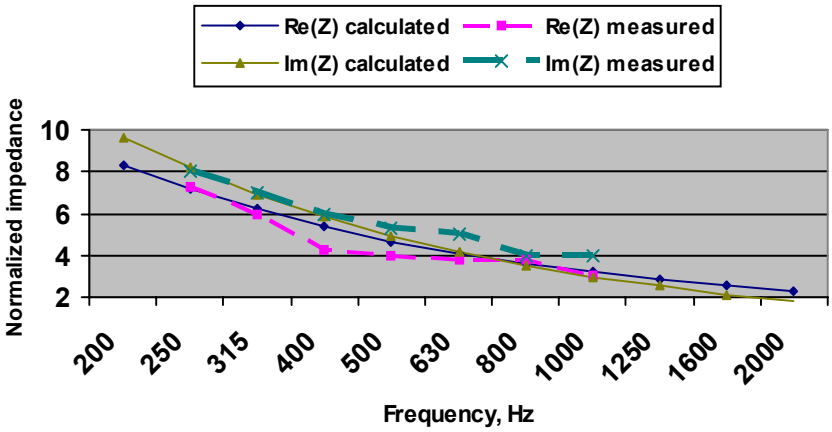

Figure 6 - The measured values of the impedance compared to calculated made in current investigations

If σ changes, the location and level of the first dip is changed, and this has a much stronger effect on the error than random noise. In Fig. 7 (figure 5.1 of the [27]) we can see that for this geometry - h_s=1.5 m, d=4 m, h_r=0.5 m (geometry is shown in Fig. 8) - the first frequency dip occurs already at 250 Hz, which means that for the higher frequencies we will have a lot of dips and peaks, so this is a bad geometry for this situation. They confirm the character of attenuation effect, but measured results at higher frequencies are seems to be overestimated.

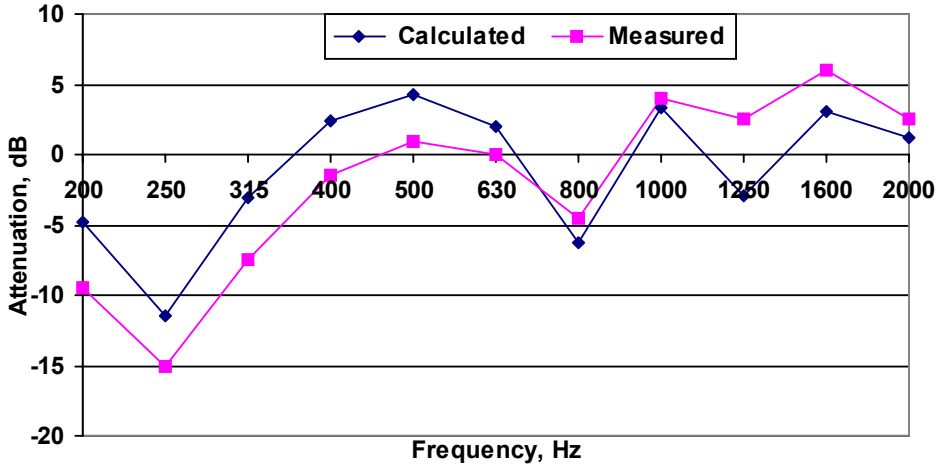

Figure 7 - Measured and calculated *SPL* of the attenuation for the same data as in fig. 5.1 of the [27]

For monopole type sources interference effect Δ*SPL* for direct and reflected sound rays in each frequency band may be defined using the following formula [28]:

$$\Delta SPL = 10\lg\{1 + (\frac{R_1}{R_2})Q^2 + \frac{2R_1}{R_2}|Q|\frac{\sin[k(R_2 - R_1)\Delta f}{k(R_2 - R_1)}\cos[k(R_2 - R_1) + \varphi]\}, \qquad (10)$$

where coefficient Q is defined from the following equation

$$Q = |Q|\exp(i\varphi) = R(\theta) + [1 - R(\theta)]E(\rho), \qquad (11)$$

with any peculiarities of the models under investigation [8-20], Δf =0,115 for 1/3-octave frequency band, k - wave number, φ - phase difference.

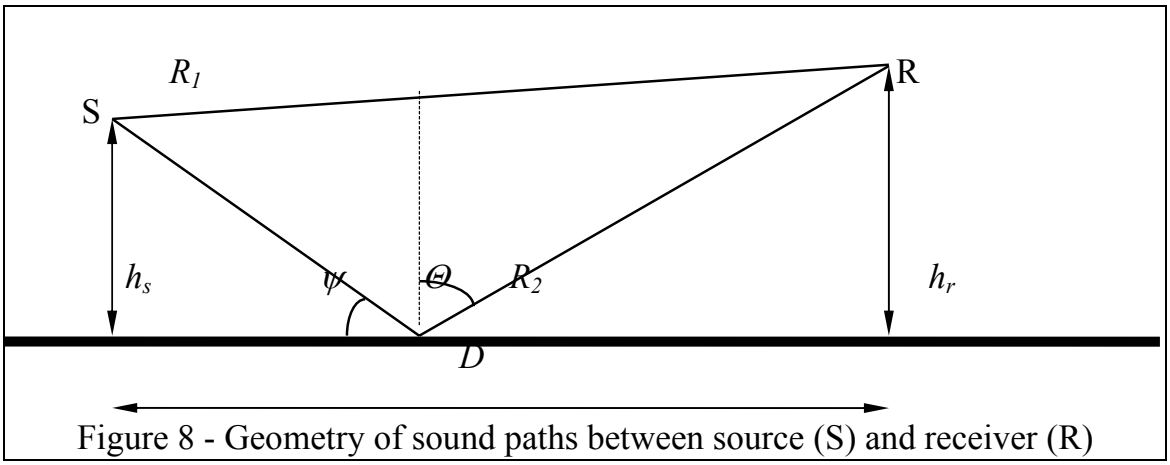

Figure 8 - Geometry of sound paths between source (S) and receiver (R)

"Loss factor" $E(\rho)$ is defined as [8-20]:

$$E(\rho) = 1 + i\sqrt{\pi}\rho\exp(-\rho^2)erfc(-i\rho), \qquad (12)$$

"numerical distance":

$$\rho = \frac{1+i}{2}\sqrt{kR_2}(Z^{-1} + \cos\theta),$$

and mathematical contrary Error function:

$$erfc(x) = 1 - erf(x) = \frac{2}{\sqrt{\pi}}\int_x^\infty \exp(-t^2)dt.$$

Sound propagation calculations scheme, proposed in [27], have been used for comparison of the models [8-20]. The geometry of the calculation scheme assumes that the point source is located on a distance D=30 m from the receiver, on the height h_s = 0,2 m above the ground, and the receiver height is h_r = 1,5 m above the ground. Three kinds of covering with flow resistivity 40, 160 and 630 *kPa s/m*^{2} have been observed in calculations. Impedance model was used in a form of 1-parameter model (6). The results of calculations for the basic model are shown in Fig. 9. These results are identical to those obtained with the analogue model and published in [27] and they confirm the reliability and accuracy of the algorithm of subroutine LATER that was written for this purposes.

Following marks are used for the main investigated models (all for monopoles): **Chi-Sor -** model [15], **Thomas** - model [13], **Rudnick -** model [11], **Kawai -** model [17], **Ingard -** model [12], **Horis** – for horisontal and **Vertic –** for vertical dipoles [19]. The results of calculated excess attenuation (EA) for σ = 630 *kPa s/m*^{2} are shown in Fig. 10. Results for monopole and horisontal dipole are absolutely equal

and lay in one curve. The results for resistivity classes $\sigma = 160$ *kPa s/m*^{2} and $\sigma = 40$ *kPa s/m*^{2} are so closed for every model.

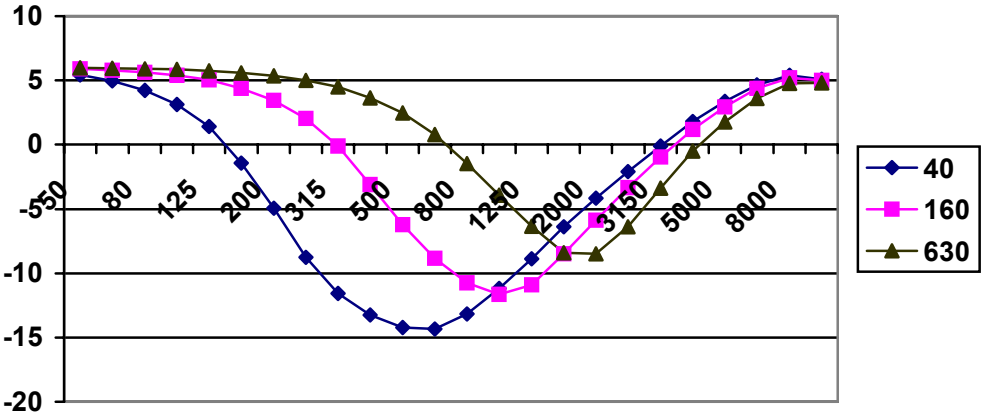

Figure 3.10 – Sound pressure level for the lateral attenuation for three flow resistivity classes ($\sigma = 40$, 160 and 630 *kPa s/m*^{2} respectively)

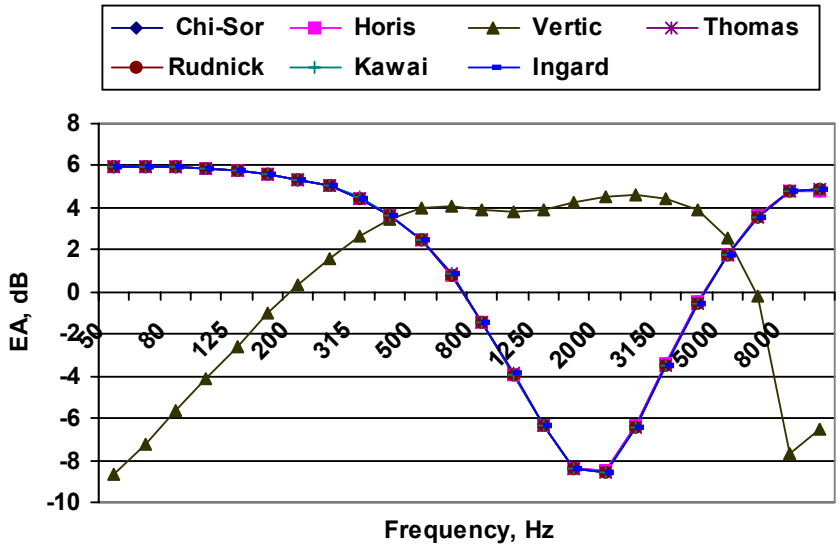

Figure 10 – Excess attenuation models comparison for $\sigma = 630$ *kPa s/m*^{2}

In paper of Parkin and Scholes [29] the results of a series of measurement of horizontal propagation of sound over an airfield were reported. The range an airfield consisted of a swatch of grass up to 5.1 cm high through grass and farmland on which gross grew up 20.3 cm high. The swatch was 304.8 m wide and 1127.8 m long.

Experimental data are compared with the predicted sound field near to ground with finite impedance using the models [8-20]. Fig. 11 compares all above mentioned models for excess noise attenuation with experimental data of Parkin and Scholes for 7 distances: model of Chien and Soroka (**LaterM**), model of Thomasson (**LaterMTH**), model of Rudnic (**LaterMRUD**), model of Kawai at al.

(**LaterMKAW**) and model of Ingard (**LaterMING**), **LaterH** - results for horizontal dipole, modeled by [19]. Specific normalized admittance is given by one-parametric model (6). Good agreement is observed between different models for all distances and at frequencies less than 6300 Hz.

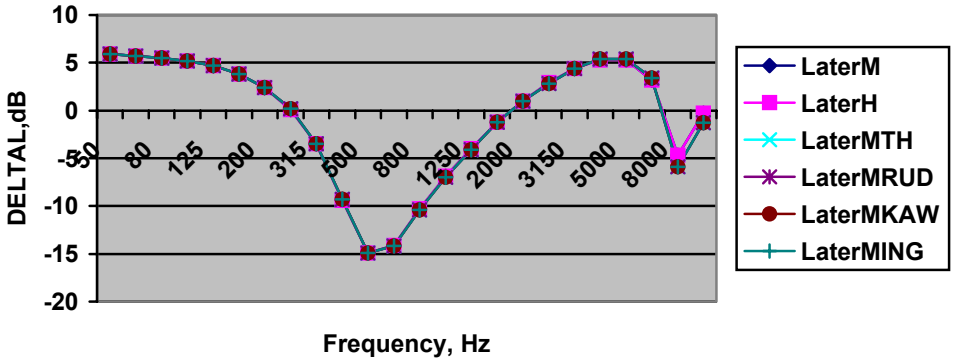

Figure 11 - Comparison of the investigated models at prescribed distances 109,73 m

4. Effects of atmosphere turbulence

In eq. (6) a coherent addition of the direct and reflected waves is assumed. However in the real atmosphere, random fluctuations of wind and temperature cause fluctuations of amplitude and phase of the sound wave. This may be transformed into measured *SPL* fluctuations of about 10 dB or more over a period of minutes.

The overall coherence coefficient F determining the coherence between two rays is the product of a number of coherence coefficients as shown in following equation:

$$F = F_f F_{\Delta\tau} F_c F_r F_{sc}, \qquad (13)$$

where F_f, $F_{\Delta\tau}$, F_c, F_r, F_{sc} are coherence coefficients corresponding accordingly to frequency band averaging, averaging due to fluctuating refraction, partial incoherence (e.g. turbulence), surface roughness and scattering zones.

A solution for F_f is given in [28] which can be expressed for one-third octave bands as shown:

$$F_f = \frac{\sin[k(R_2 - R_1)0.115]}{k(R_2 - R_1)0.115},$$

and it is utilized in eq. (10).

A similar solution can be obtained for fluctuating refraction $F_{\Delta\tau}$, for a fixed wave number k if it is assumed that the travel time difference τ_2-τ_1 is varying within the range $\Delta\tau_2$-$\Delta\tau_1$ and is uniformly distributed within this range. τ_1 is the travel time corresponding to the primary ray and τ_2 to the secondary ray:

$$F_f = \frac{\sin[\pi(\Delta\tau_2 - \Delta\tau_1)f]}{\pi(\Delta\tau_2 - \Delta\tau_1)f}.$$

A somewhat complex method for estimating the effect of atmospheric turbulence is proposed in [30]. However, the accuracy of this method is not known,

and on this background a more simple empirical proposal [26] is under consideration as shown in following equation with turbulence parameter η - the mean square fluctuation of the index refraction or the refraction fluctuation index:

$$F_c = \exp\{-[\eta k(R_2 - R_1)]^2\}. \qquad (14)$$

Outside the shadow area, the rapid fluctuations of wind and temperature modify for a while the speed of each sound ray and, as a consequence, its phase and amplitude. Thus, the turbulence effect is maximum, where interference predominates. Daigle [31] developed a model using a factor of partial correlation Γ (or T for Gaussian turbulence spectrum) based on meteorological parameters, such as the turbulence scale L_T, the separating distance between rays ρ and the refraction index $\overline{\mu}^2$.

For a spherically symmetric source having unit pressure at 1 m the mean-squared received pressure is given by [32]

$$\overline{p}^2 = \frac{1}{r_d^2} + \frac{|F|^2}{r_r^2} + \frac{2|F|}{r_r r_d}\cos[k(r_r - r_d) + \theta]T,$$

where $T = \exp[-\sigma^2(1-\rho)]$, σ^2 is the variance of the phase fluctuation along the path, ρ is the phase covariance between path, $F = |F|\exp(i\theta)$ is the complex spherical wave reflection factor, k is the wave number as usual. The factor σ^2 is given by

$$\sigma^2 = \frac{\sqrt{\pi}}{2}\overline{\mu}^2 k^2 L L_0, \quad for\ L > kL_0^2,$$

where $\overline{\mu}^2$ is the variance of index of refraction, L is the horizontal path length, L_0 is the Gaussian turbulence scale. The phase covariance between path is given by

$$\rho = \sqrt{\pi}\frac{L_0}{2h} erf(\frac{h}{L_0}),$$

where h is the maximum path separation, $erf(x)$ is an Error function (see (3.2)).

In general for the mean-squared pressure one can obtain

$$\overline{p}^2 = \frac{\rho c W}{4\pi}\{\frac{1}{r_d^2} + \frac{|F|^2}{r_r^2} + \frac{2|F|}{r_r r_d}\cos[k(r_r - r_d) + ArgF]\Gamma\}, \qquad (15)$$

with function Γ defined as:

$$\Gamma(R,\rho) = \exp\{\frac{\sqrt{\pi}}{2}\overline{\mu}^2 k^2 L_T[1 - \varphi(\frac{\rho}{L_T})\frac{\rho}{L_T}]\},$$

where

$$\varphi(\frac{\rho}{L_T}) = \int_0^{\rho/L_T}\exp(-t^2)dt.$$

In practice, scale L_T is generally close to 1 m, and the refraction indices $\overline{\mu}^2$ range from 10^{-7} for cases with small turbulence to 10^{-5} when the turbulence is strong. The results presented in [32] showed that theoretical results were best correlated with experiments when the separating distance between rays ρ was chosen as the half of the maximum separation. This solution only applies when the refraction is weak, that

is for the case with only one direct and one reflected ray. It cannot be used when strong negative refraction exists or when the receiver lies in the shadow area [33].

Fig. 12 compares the result of calculation using different values of variance of the phase fluctuation σ for some distances from source to receiver and neutral weather condition [29]. Good agreement between experimental data and calculated results was obtained for the phase fluctuation σ between $2 \cdot 10^{-7}$ …$7 \cdot 10^{-7}$.

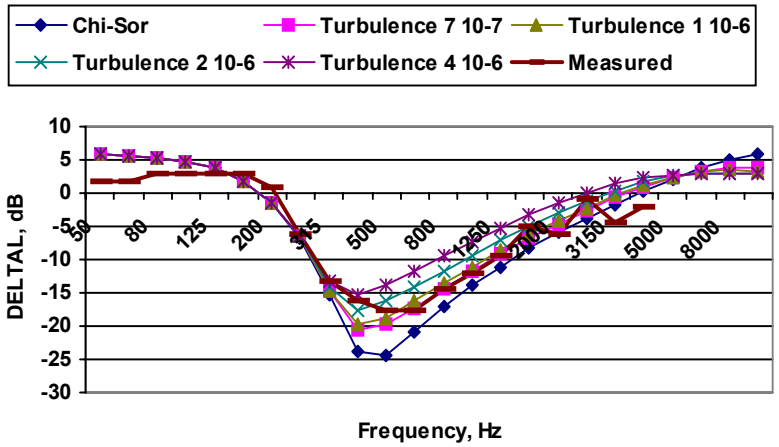

a)

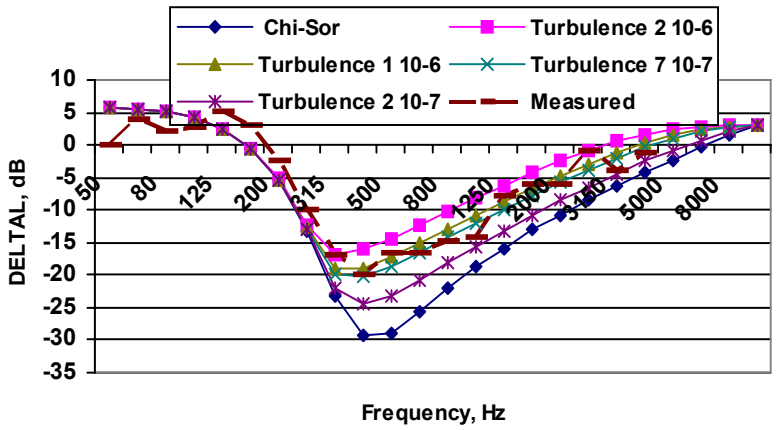

b)

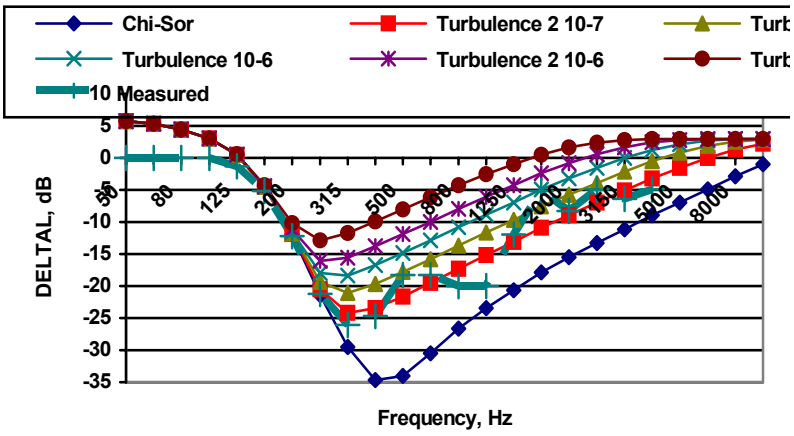

c)

Figure 12 - Predicted SPL attenuation for different phase fluctuations and distances from source to receiver: a) 347,47 m, b) 615,7 m, c) 1097,28 m

5. Refracting atmosphere

An assumption of heuristic approach that there are many sound rays exist in a refracting atmosphere near impedance ground may and be reflected from surface and added in point of receiver. For short ranges the angle of incidence of the reflected ray and the length of both the direct and the reflected ray will change in comparison to the homogeneous case. Every ray may contribute to the noise level at the point of receiver including the influence of every reflection along the particular ray.

How much of the possible reflected rays in refracting atmosphere may reach the receiver point - is a task of probability theory. In any case the total effect of the sound refraction in air may be described by the bounds: minimum - if only one reflected ray reaches the receiver; maximum - if all the predefined reflected rays reach the receiver, but this case is quite impossible in real situation.

For comparison of Parkin and Scholes' measurement data [29] and calculated results for temperature lapse conditions two cases for distances 347.47 m (Fig. 13)) from source to receiver are considered. There was assumed that shadow zone for receiver point is absent (proved by calculation), it means that receiver point in illumination zone. For larger distances, more than 615.7 m, the shadow zone covers the receiver point and appropriate sound propagation model must be used for calculation in such cases.

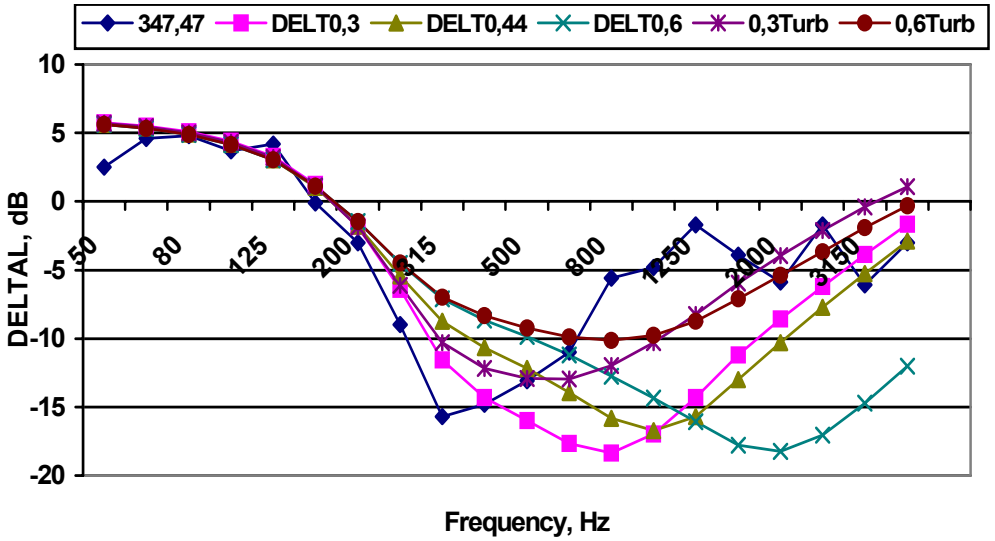

Figure 13 - Third-octave spectra for noise attenuation at distance 347.47 m for the temperature difference between heights 1.22 and 12.2 m equal to -0.3 ^{0}C (**DELT0,3**), -0.44 ^{0}C (**DELT0,44**), -0.6 ^{0}C (**DELT0,6**) accordingly. The lines **0,3Turb** and **0,6Turb** represent calculated cases with turbulence effects defined by refraction index equal to $2 \cdot 10^{-6}$ and for the temperature difference (between the heights 1.22 and 12.2 m) -0.3 ^{0}C and -0.6 ^{0}C respectively

At distance 347.47 m for temperature difference between heights 1.22 and 12.2 m equal to -0.3 ^{0}C and variance of the refraction index equal to $2 \cdot 10^{-6}$ are in a good compliance with Parkin and Scholes' experimental data. At distance 615.7 m best

compliance is observed for temperature difference -0,2 ^{0}C and variance of the index refraction $2 \cdot 10^{-6}$.

Fig. 14 shows that experimental and computed spectra are in good quantitative agreement between themselves in next condition: the temperature difference between heights 1.22 m and 12.2 m is equal to 0.38 ^{0}C, reflected rays with point of sound reflection closest to the point of reflection of the ray in homogeneous conditions, for example equal to 267.49 m is best fitted to measured data, particularly over the range of frequencies below 2500 Hz.

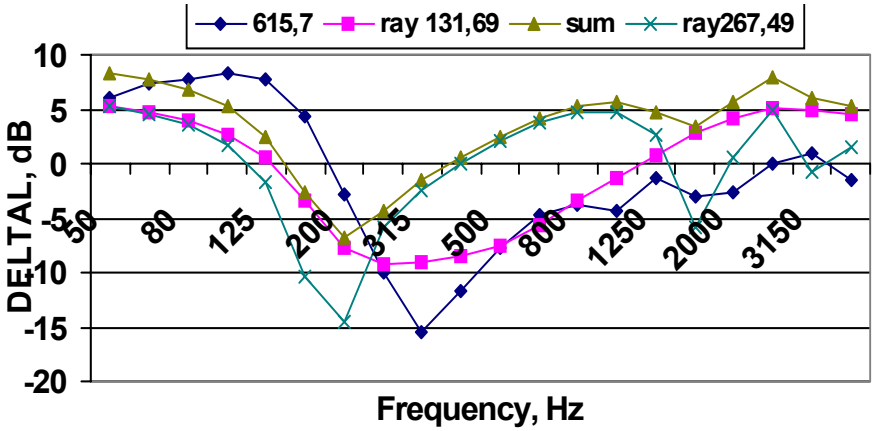

a)

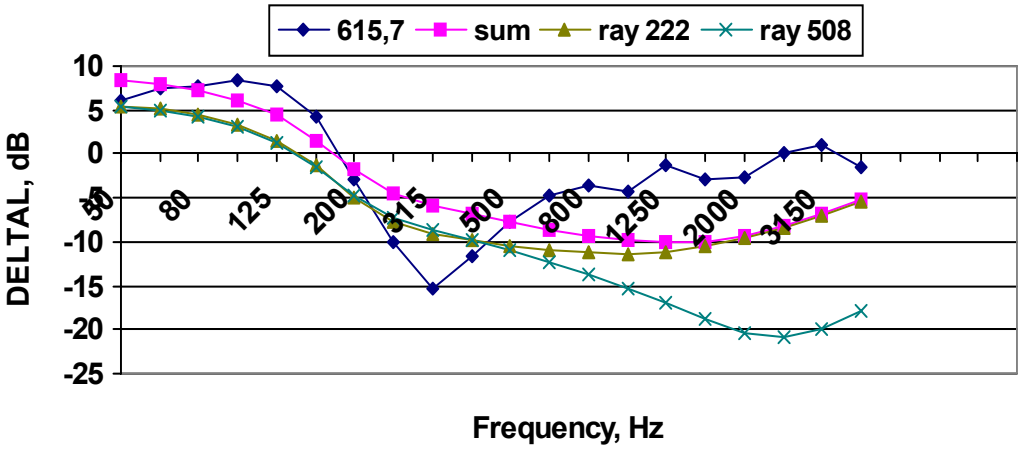

b)

Figure 14 - Third-octave spectra of attenuation at a distance 615.7 m for one and two rays models: a) points of reflection sound rays - 222 m, 508 m, the temperature difference between 1.22 m and 12.2 m is 0.3 ^{0}C; b) points of reflection sound rays - 131.69 m, 267.49 m, the temperature difference between 1.22 m and 12.2 m is 0.38 ^{0}C

The atmosphere will never be perfectly stable, more or less containing variations in the vertical sound speed profile, leading to fluctuating refraction. Even when the average refraction corresponds to the straight line propagation this effects will be seen [35]. A similar solution can be obtained for fluctuating refraction $F_{\Delta v}$ for

a fixed wave number k if it is assumed that the travel time difference τ_2-τ_1 is varying within the range $\Delta\tau_2$-$\Delta\tau_1$ and is uniformly distributed within this range [35]:

$$F_f = \frac{\sin[\pi(\Delta\tau_2 - \Delta\tau_1)f]}{\pi(\Delta\tau_2 - \Delta\tau_1)f}, \qquad (16)$$

where τ_1 is the travel time corresponding to the primary ray and τ_2 to the secondary ray.

For maximum conditions of sound propagation during the aircraft noise assessment in noise control points under the flight path wind or temperature refraction provides only direct and one reflected rays, modifying in comparison with homogeneous case the grazing angle, the phase and transmission loss of the effect.

For example, during flight testing of the Airbus-321 noise at take-off/climbing few points of noise control were located on both sides from flight path, some of them symmetrically one to another. Displacement of the side point of noise control is equal to 450 m, all symmetrical to point on centerline, abscissa of all the control points is equal to ~942 m, height of the microphone over the ground is equal to 1.2 m.

For non-refracting atmosphere and for slant distance R_0= 450.00 m, direct ray length R_1= 475.56 m, reflected ray length R_2= 476.34 m, reflection point = 446.54 m, grazing angle = 19.1 deg. For refracting atmosphere and for slant distance R_0= 450.00 m, direct ray length R_1= 478.94 m, reflected ray length R2 = 479.72 m, reflection point = 447.98 m, grazing angle = 30.8 deg.

Chien and Soroka model for monopole provides the attenuation shown in Fig. 15. First dip is concentrated at the frequency band 200 Hz. In noise measurement in first dip is located in the same band 200 Hz too, second dip - in band 800 Hz and the same was observed in measurements. But the calculated dip is more vivid, that is understandable taking in mind the total coherence approach of the model used for lateral attenuation in this case. In refraction case grazing angle becomes larger than in homogeneous thus lateral attenuation is less vivid than in homogeneous case.

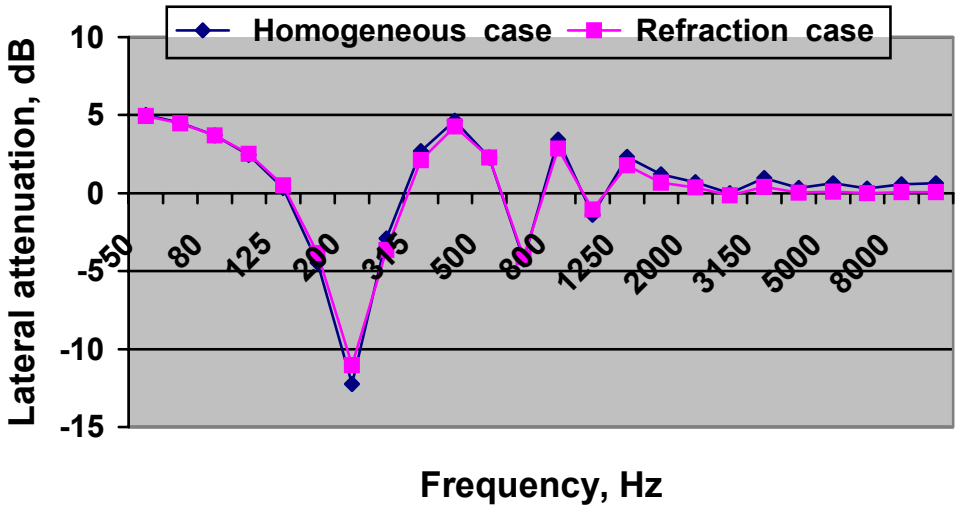

Figure 15 - Lateral attenuation for the refraction and homogeneous cases

6. Wing shielding effect model

Experimental investigations [36] have shown that wing shielding can have a measurable effect on the attenuation of engine inlet and/or exhaust noise, for certain engine mount configurations. This is an important consideration for noise predictions for business aircraft with aft-mounted engines.

The developed wing-shielding model employs the Fresnel diffraction theory for a semi-infinite barrier, as described in [37], modified for the finite barrier, as the aircraft wing may be presented. The process for computing the attenuation resulting from wing shielding is described in the way similar to [38]. As an initial step, the wing configuration is described in a local co-ordinate system with the origin positioned at the engine inlet (point 1), as shown in Fig. 16. Then, the local origin and wing co-ordinates are transformed into a global co-ordinate system consistent with the observer location on the ground. This transformation must take into account the aircraft attitude and position at the particular time of the observation.

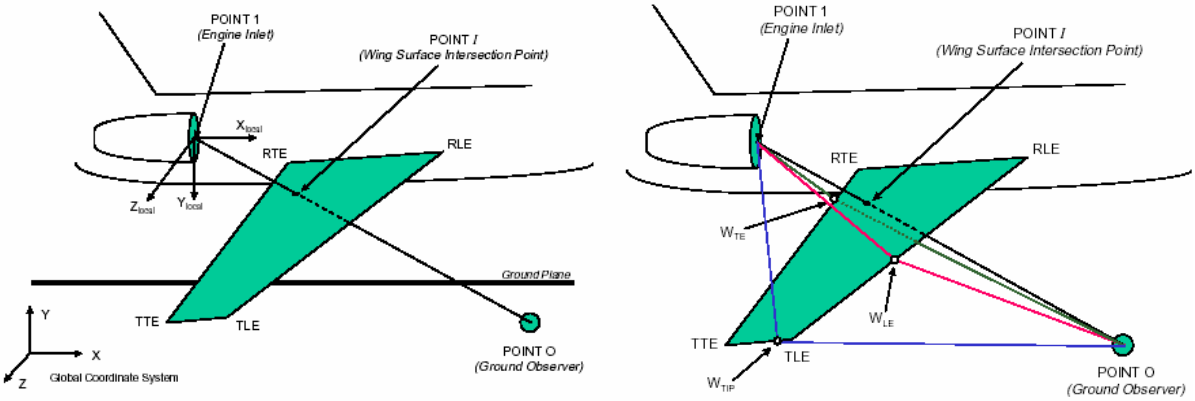

Figure 16 - Definition of the wing-engine-observer configuration with local and global co-ordinate systems for the wing-shielding model and character distances for wing diffraction assessment [38]

From all three possible distances (Fig. 16) the difference in source-receiver path length between the direct and diffracted sound fields may be computed:

$$\delta = (d_{1W} + d_{WO}) - d_{1O}\,, \qquad (17)$$

where $\delta > 0$ when point *I* lies on the wing surface, $\delta = 0$ when point *I* lies on the wing boundary edge, and $\delta < 0$ when point *I* is beyond the wing surface. From this difference in distances, the Fresnel number is calculated as follows:

$$N = 2 f_i \delta / c, \qquad (18)$$

where f_i represents the frequency for each 1/3 octave band, in Hz, and c is a speed of sound in free stream. The attenuation equation is then computed for each 1/3 octave band frequency as follows:

$$\begin{aligned} \Delta L &= 5 + 20\lg\left(\sqrt{2\pi N}/th\sqrt{2\pi N}\right) && \text{for } 0 \le N \le 100; \\ \Delta L &= 5 + 20\lg\left(\sqrt{2\pi |N|}/th\sqrt{2\pi |N|}\right) && \text{for } 0.2 \le N < 0; \\ \Delta L &= 0 && \text{for } N > 0.2. \end{aligned} \qquad (19)$$

Equations (19) are well-known Maekawa solutions [37]. For $N<0$ another approximation may be proposed [39]:

$$\Delta L = 1{,}1518211\ \exp[0{,}5493061(N+3)] - 1{,}1468337 \quad \text{for} \quad -3 \le N < 0.$$

In order to obtain an equivalent total attenuation from the combined effects of the three diffraction edges, the individual attenuation at any frequency f_i are combined as follows:

$$A_{TOT} = -10 \log \sum 10^{-(A_k/10)} \qquad (20)$$

where k = LE, TE, TIP (three edges under consideration).

Calculations of diffraction (screen) effect of the wing for sound propagated from the engine installed at the tail of the aeroplane have been done for the scheme of Yakovlev-40, which has 3 engines in the power plant - 1 over the fuselage and 2 aside of the fuselage. Side engines are mounted in a such way, that their flow intakes are over the wing on a length $\mathrm{Delx_{WE}}$ = 0.25 m along the wing chord at engine half-span z_{EN}. The vertical displacement of the intakes over the wing $\mathrm{Dely_{WE}}$ = 1.2 m is too small, so the diffraction effect must be sufficient. Calculated influence on the *OASPL,* L_A and *PNL* for this case (noise spectrum of the engine fan is equal to by-pass engine with ratio m=2.5 like for AI-25 engines of Yakovlev-40) are following: 8.3 dB, 10.5 dBA and 10.3 PNdB (for fan noise separately).

Because of quite small by-pass ratio of the engine under the consideration the contribution of fan noise in total spectrum of the aeroplane is not so huge and the resulting influence of the wing shielding on the total aeroplane noise is much less then for fan noise alone.

The influence of the shielding of fan noise has been analyzed for flight noise level, particularly for approach flight of the Yakovlev-40. Results of the noise calculation (*PNL* and L_A) at noise control point No 3 (2000 m before the runway edge) are shown in Fig. 17, where noise levels calculated without (*PNL* and L_A) and with (PNL_{shield} and $L_{Ashield}$) sound shielding are dependent of distance along glide-path. Found before maximum screen effect ~5PNdb and ~3dBA are presented in flight event (at distances -2200…-2150 m) and their influence on flight event indices are following: $\Delta EPNL$ = 2.4 EPNdB, ΔL_{AMAX}= 2.0 dBA, $\Delta PNLTM$ = 2.0 PNdB, where for flight without sound shielding by wing:

EPNL= 97.8 EPNdB, L_{AMAX}= 87.8 dBA, *PNLTM*= 103.9 PNdB,

and for flight without sound shielding by wing:

EPNL= 95.4 EPNdB, L_{AMAX}= 85.8 dBA, *PNLTM*= 101.9 PNdB.

Analysis of the result show that at the moment t of the flight, when *PNL=PNLM*, shielding effect ΔPNL is less then at distances -2200…-2150 m, because intersection point I in latest situation is placed strictly in the middle of the chord of the wing thus providing maximum effect of the shielding. Spectral effect qualitatively and quantitatively is the same as in ANOPP calculations [38].

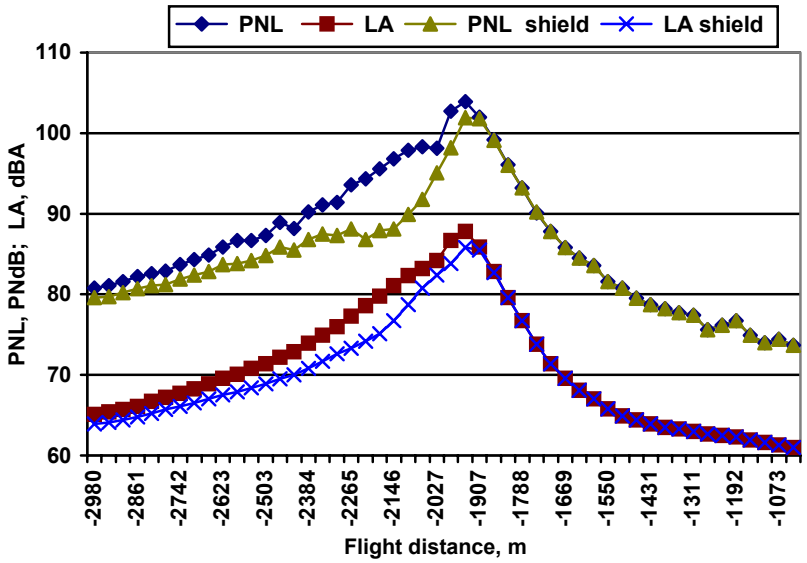

Figure 17 - Glide-path noise event of Yakovlev-40 in dependence with flight distance (point -2000 m is a point of noise control)

7. Sound shielding by fuselage

When acoustical waves are spreading out, for instance, from jets or fans some of them are deflected and/or shielded by fuselage. There are scattered waves produced in this case. Scattered waves may spread out from the fuselage in all directions, distorting and interfering with incident waves.

If we consider the scheme in which two point sources (like two engines on the sides of the fuselage) with volume velocity Q are set on the surface of the cylinder. In this case the sound pressure is defined as ($kR >> 1$) [40]

$$p(R,\varphi,\beta) = \frac{Q\rho_0 c}{2\pi^2 a\cos\beta}\frac{\exp[ik(R - z_0\sin\beta)]}{R}\sum_{n=0}^{\infty}\varepsilon_n(-i)^n\frac{[\cos n(\varphi-\varphi_1)+\cos n(\varphi-\varphi_2)]}{H_n^{(1)\prime}(ka\cos\beta)} \quad (21)$$

The model of noise shielding by fuselage (cylinder surface), that was by eq. (21), is analysed here numerically. Maximum interest may be supposed for directivity pattern (Fig. 18) of the effect (absolute value is defined by expression (21)):

$$R(\varphi) = \left|\frac{p_0(\varphi)}{p_0(\varphi_1)}\right|,$$

where one source is considered at opposite side to receiver point, thus $\varphi_1 = 0$.

8. Sound refraction by jets

Sound refraction is produced by impedance difference of the medium of sound propagation [41]. Jets from the engines may produce such a difference due to temperature and velocity of the jet. The approach of the Ostashev (3.4) [41] has been used for numerical analysis and it was compared with simple formula of the assessment of noise transmission coefficients known from classical acoustics.

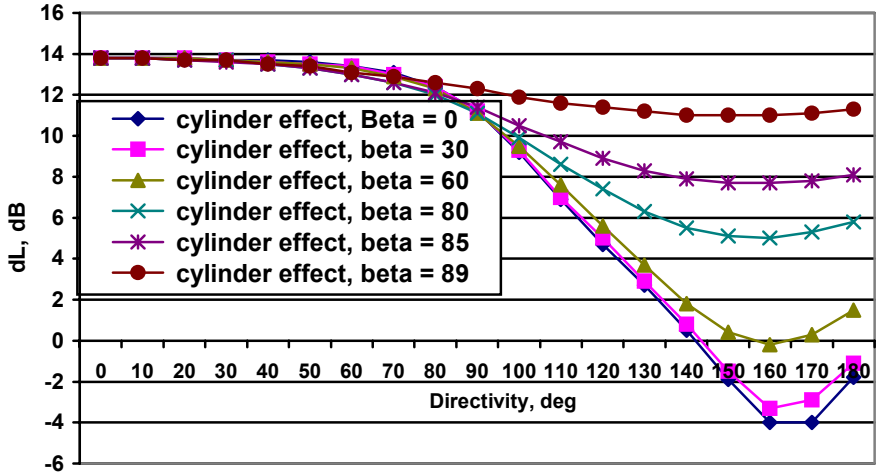

Figure 18 - *OASPL* reduction due to the cylinder shielding in dependence with β, a=2m

The coefficient of the sound wave transmission through the layer can be expressed in the form [41]

$$W = \frac{4Z_2Z_3}{(Z_2 - Z_1)(Z_3 - Z_2)\exp(iq_2d) + (Z_2 + Z_1)(Z_3 + Z_2)\exp(-iq_2d)}, \quad (22)$$

where Z_i is the impedance of a moving media, $q_2 = atg\theta_2$. From above equation it follows that the dependence of the transmission coefficient W on the thickness d of the layer and the vertical wave-number $q_2 = atg\theta_2$ has an oscillatory character.

In case $v_1 \neq 0$, $v_3 \neq 0$

$$Z = \frac{\rho c}{\sin\theta(1 + \cos\theta e \cdot v/c)}.$$

For simple case, without dependence of impedance from frequency, the problem considered above is reduced to that of plane wave reflection by an interface between moving media, in this case

$$W = 4\ Z_2\ Z_3/[(Z_3 + Z_2)\ (Z_2 + Z_1)], \quad (23)$$

where $Z_i = \frac{\rho_i c_i}{\sin\theta_i}$ for $v_1 = v_2 = 0$.

A frequency dependence of the refraction effect, produced by jets of the engine working on descending mode, are presented in the Fig. 19. If we compare the frequency dependent transmission coefficient (22) with derived from the classical formula (23) W_{trans} = 0.85, we may find that averaged along the frequency range value is equal to classical result.

Such dependence of the transmission coefficient may result on sound reflection effect if the reflected ray is passing through the exhausting jet like shown in Fig. 20. Example of the dependence is represented in Fig. 21. Reflection effect is calculated in accordance with the model [15].

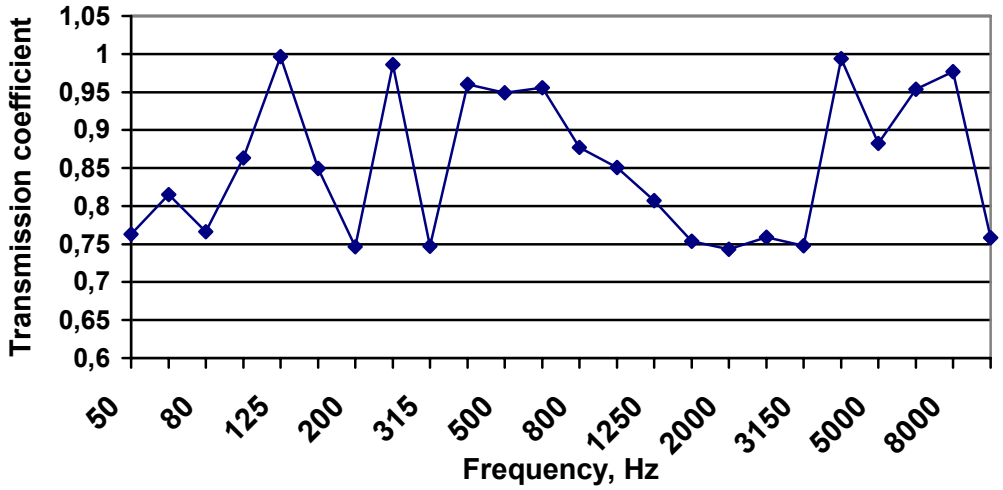

Figure 19 - Sound transmission coefficient for the engine jet in descending flight mode

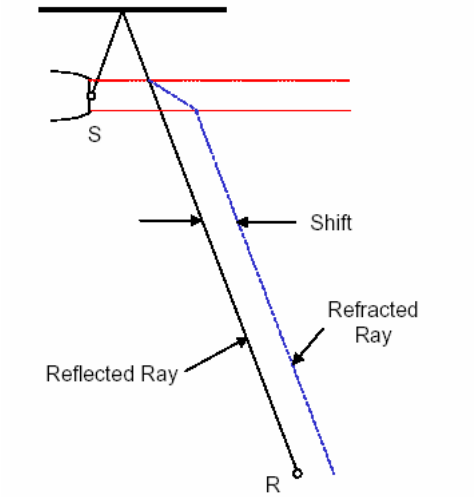

Figure 20 - A reflected ray experiences refraction as it passes through the exhaust jet [42]

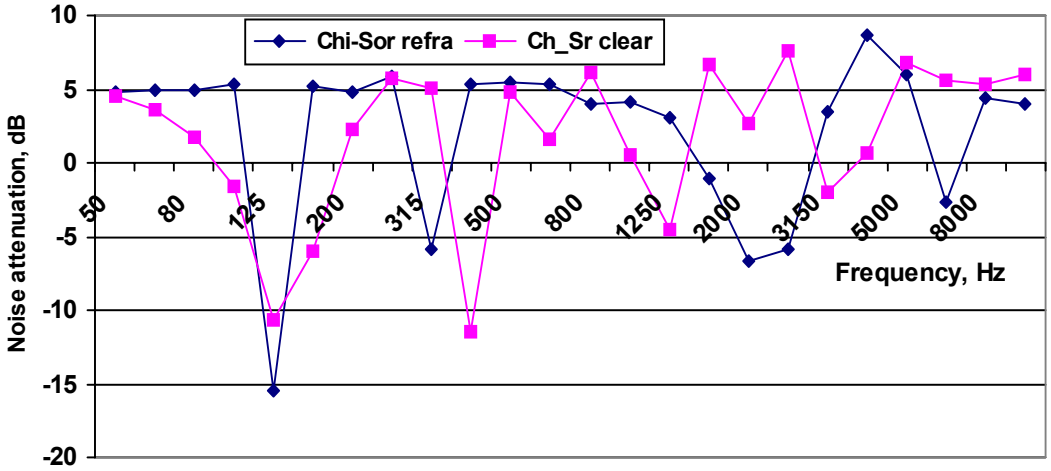

Figure 21 - A reflection effect influenced by refraction as the ray passes through the exhaust jet

9. Sound reflection by wing

Sound reflection by wing was considered in a same manner as sound shielding in sub-part 6. The results were obtained for distance 100 m (~equal to the distance for approach noise control point) for linear *OASPL*, L_A and *PNL*. The method for the preparation of the output noise results is as follows:

1. Obtain the geometry and received spectra data from the input files. The reflecting panels that represent the wing/flap system are modelled as planar surface.
2. For each reception time value, calculate the point *W* and determine if the ray intersects the object of sound reflection.
3. Compute the sound effects at the desired values of frequency using the model prescribed in sub-part 3, but for much more hard surface, thus for high values of σ.
4. Apply the amplification (or attenuation) to the appropriate value of the received mean-square pressure.

All the results were obtained using the models and subprogram developed specially for current investigation. Noise indices for analysed flight event were defined for the aircraft like Yakovlev-40, but the engines installed under the wing, with next values:

- without reflection and refraction

  $EPNL$= 99.7 EPNdB, L_{AMAX}= 87.0 dBA, $PNLT_{MAX}$= 102.4 PNdB;
- with reflection, no refraction

  $EPNL$= 101.3 EPNdB, L_{AMAX} = 91.0 dBA, $PNLT_{MAX}$ = 106.7 PNdB;
- with reflection and refraction (like in Fig. 20)

  $EPNL$= 102.0 EPNdB, L_{AMAX} = 91.0 dBA, $PNLT_{MAX}$ = 108.1 PNdB.

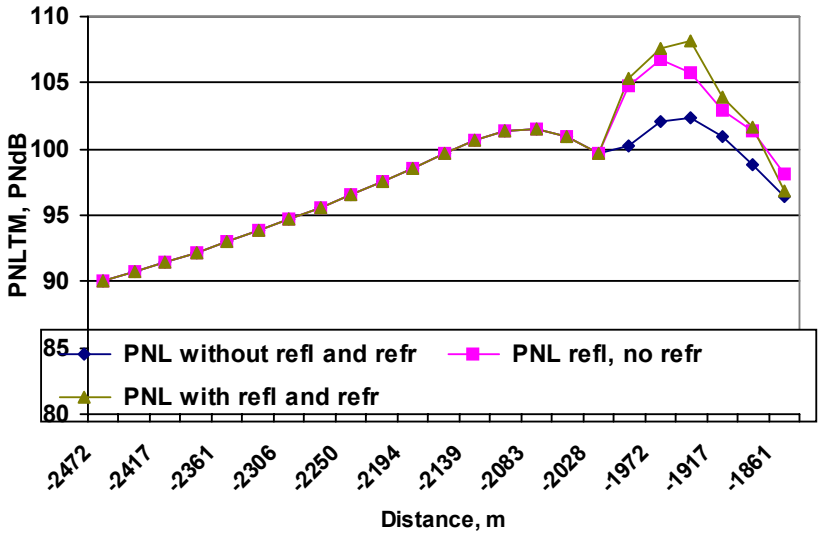

Figure 22 - Comparison for noise assessment without reflection and refraction, for sound reflection alone and for their both influence

Measurements of mentioned above noise generated by Airbus 321 allow to observe the effect of sound reflection by wing analysing the behaviour of fan discrete tones. For example, at landing noise measurements such a band may be a 1600 Hz

1/3-octave band (nicely observed in most part of the spectra for landing noise), inside which a 1-st harmonics of the fan rotor discrete tone exists (it's value is little bit more than 1700 Hz, so sometimes the energy of this harmonics may transport to near 1/3-octave band - 2000 Hz). In Fig. 23 (measured) and 24 (calculated) the flight noise events (SPL as a function of flight time) for SPL of the 1600 Hz 1/3-octave band are shown. Dips at points (moments) 16-17, 26-27, 46-47, 53-54 are observed at every event - measured or calculated in a same manner, they are produced by interference effects of direct and reflected wave from the surface covering and they confirm the validity of the lateral attenuation models used in current investigations. But more interesting to investigate the pick level of these events - the comparison of calculated noise events with and without impact of possible sound rays reflected by wing in Fig. 24 show that just that effect may describe the existance of such picks.

Figure 23 - Flight noise event for SPL at 1/3-octave band 1600 Hz (measurements) at measurement point No A2

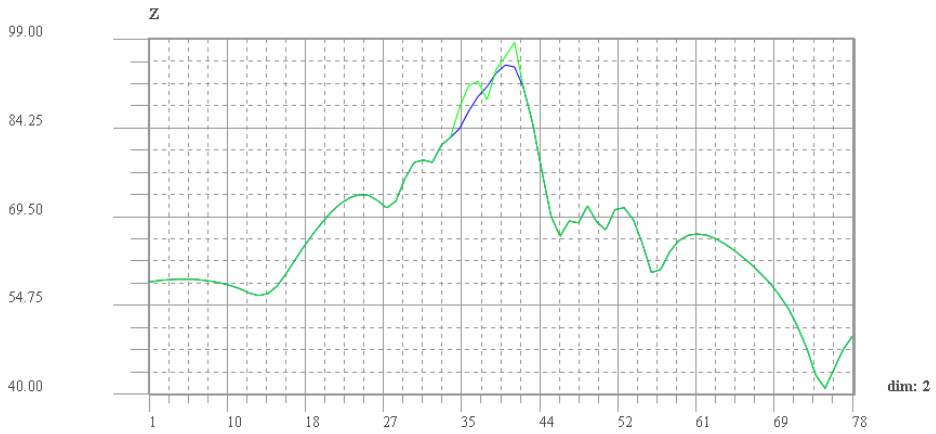

Figure 24 - Flight noise event for SPL at 1/3-octave band 1600 Hz (calculations) at measurement point No A2: **blue line** - SPL without impact of the ray reflected by wing; **green line** - SPL with impact of the ray reflected by wing

Conclusion

All the prediction procedures are based on theoretical solutions of wave equation, semi-empirical models, engineering methods, which use reasonable physical arguments.

For all the analyzed models the numerical algorithms are implemented in appropriate subprograms, written in Fortran and included in specialized library. They were analyzed for the sound propagation and engine installation influence for particular types of the aircraft, results of which confirm the necessity of their usage in aircraft noise calculation.

References

1. Zaporozhets O., Tokarev V. Aircraft noise modelling for environmental assessment around airports // *Applied Acoustics*, vol. 55, No 2, 1998, pp. 99-127.
2. Recommended Method for Computing Noise Contours Around Airports. - Montreal: ICAO, Circular 205 AN/1/25, 1988. - 25p.
3. ISO 9613-1:1996. Acoustics - attenuation of sound during propagation outdoors- Part 1: Calculation of the absorption of sound by the atmosphere
4. IEC 1094-3, 1995: Measurement microphones - Part 3: Primary method for free-field calibration of standard laboratory microphones by the reciprocity technique.
5. ANSI S1-26-1995 Method for the calculation of the absorption of sound by the atmosphere.
6. 14 CFR Part 36 Appendix A - Aircraft noise measurement and evaluation, AC36-4C, 2000.
7. H.E. Bass, L.G. Sutherland, A.J. Zuckerwar, D.T. Blackstock, and D.M. Hester, "Atmospheric Absorbtion of Sound: Further Developments"*, J. Acoust. Soc. Am., Vol 97, 1995, pp. 680-683.*
8. Sommerfeld A. *Annalen der Physik* **28,** 665-736 (1909).
9. Van Der Pol B. Theory of the reflection of the light from a point source by a finitely conducting flat mirror, with an application to radiotelegraphy // *Physica* **2**, 843-853 (1935).
10. Norton K.A. The propagation of radio waves over the surface of the earth and in the upper atmosphere. Part 2 // *Proceedings of the Institute Radio Engineers* **25,** 1203-1236 (1937).
11. Rudnic I. The propagation of an acoustic wave along a boundary // *JASA* **19**, 348-356 (1947).
12. Ingard U. On the reflection of a spherical sound wave from an infinite plane // *JASA* **23**, 329-335 (1951).
13. Thomasson S.I. Reflection of waves from point source by an impedance boundary // *JASA* **59**, 780-785 (1976).
14. Wenzel A.R. Propagation of waves along the impedance boundary // *JASA* **55**, 956-963 (1974).

15. Chien C.F., Soroka W.W. Sound propagation along an impedance plane // *JSV* **43** (1), 9-20 (1975).

16. Attenborough K. et al. Propagation of sound above a porous half-plane // *JASA* **68** (5), 1493 -1501 (1980).

17. Kawai T., Hidaka T., Nakajama T. Sound propagation above an impedance boundary // *JSV* **83** (1) 125-138 (1982).

18. Hu Z., Bolton J.S. Sound propagation from arbitrary oriented multi-pole placed near a plane, finite impedance surface // *JSV* **170,** 637-666 (1994).

19. Kai Ming Li, Sharam Taherzaden, Keith Attenborough. Sound propagation from a dipole source near an impedance plane // *JASA* **101** (6), 3343-3352 (1997).

20. Kai Ming Li and Sharam Taherzaden. The sound field of an arbitrary oriented quadrupole near ground surfaces // *JASA* **102** (4), 2050-2057 (1997).

21. Токарев В.І., Запорожець О.І. Дослідження впливу імпедансної поверхні на розповсюдження акустичних хвиль // *Вісник НАУ* (Proceedings of the National Aviation University). – 2002. – № 1. - С.240–244.

22. Запорожець О.І., Голембиевский Г.Г. Влияние эксплуатационных факторов на уровни авиационного шума // *Вісник КМУЦА* (Proceedings of the Kyiv International University of Civil Aviation). – 2000. - № 3-4. - С.296–301.

23. Zaporozhets O., Tokarev V., Attenborough K. Predicting noise from aircraft operated on the ground // *Applied Acoustics*. – 2003. – vol.64, № 10. - P.941–953.

24. M. Delaney and E. Bazley. Acoustical properties of fibrous absorbent materials // Applied Acoustics, Vol 3, 1970. -P. 105-116.

25. Attenborough K. Natural noise control // Inter-Noise 96': Proceedings of 25th Anniversary Congress, Liverpool, 1996. - p. 51-73.

26. Attenborough K., Waters-Fuller T., Li K.M., Lines J.A. Acoustical properties of farmland. // *J. Agric. Engng res*. – 2000. – vol. 76. – P.183-195.

27. M. Ögren, H. Jonasson. Measurement of the acoustic impedance of ground. KFB project 1997-0222, Nordtest project 1365-1997, SP REPORT 1998:28 Acoustics Borås 1998.

28. Chessell C.I., Propagation of noise along a finite impedance boundary // *J. Acoust. Soc. Am.* – 1977. - Vol. 62, pp. 825-834.

29. Parkin P.H., W.F. Scholes The horizontal propagation of sound from a jet engine close to the ground at Hatfield // *J. Sound Vib*. – 1965. – vol **2**(4). - P. 353-374.

30. L'Espérance A. et al., Heuristic model for outdoor sound propagation based on an extension of the geometrical ray theory in the case of a linear sound speed profile // *Applied Acoustics*, - 1992 -Vol. 37, - P. 111-139,.

31. G. A. Daigle Effects of atmospheric turbulence on the interference of sound waves above a finite impedance boundary // *JASA* – 1979. – vol. **65**(1), - P. 45-49.

32. Raspet R. and W. Wu, "Calculation of average turbulence effects on sound propagation based on the fast field program formulation", JASA **97**(1), 147-153 (1995).

33. Daigle G.A., Piercy J.E., Embleton T.F.W.. Effects of Atmospheric Turbulence on the Interference of Sound Waves Near a Hard Boundary // J. Acoust. Soc. Am., Vol. 64, n°2 1978.

34. Ögren M. Multi reflected rays in a refracting atmosphere // Nord 2000 Progress report, SP Technical Note 1999:28, Physics and Electrotechnics, Borås 1999.

35. Plovsing B., Kragh J. Prediction of sound propagation in an atmosphere without significant refraction // Delta acoustics & vibration Journal No 1818, 1998.

36. Hellstrom G. Noise Shielding Aircraft Configurations, A Comparison Between Predicted and Experimental Results *// ICAS* Paper No. 74-58, 1974.

37. Maekawa Z. Noise Reduction by Screens // *Memoirs of the Faculty of Engineering*, Kobe University, Japan, vol. 12, 1966, pp. 472-479.

38. Lysbeth Lieber. Small Engine Technology (SET) - Task 13. ANOPP Noise Prediction for Small Engines. Jet Noise Prediction Module, Wing Shielding Module and System Studies Results // NASA/CR-2000-209706, AlliedSignal Engines and Systems, Phoenix, Arizona, 2000.

39. Zaporozhets O., Tokarev, V.I., Shylo, V.F. Influence of impedance characteristics of the reflecting surfaces on reduction of aviation noise by screens // *Proceedings of 4-th Int. Congress on Sound and Vibration*, St.Petersburg, vol. 2, 1996, p.1135-1140.

40. Токарев В.І., Запорожець О.І., Голембієвський Г.Г. Дослідження розрахункових моделей впливу ефекту встановлення двигунів на рівні шуму літака // *Вісник НАУ* (Proceedings of the National Aviation University). – 2003 – № 3-4. с. 113-118.

41. Ostashev, V. E. *Acoustics in moving inhomogeneous media*, E& FN SPON, London,1997.

42. L. Lieber, D.Brown. Small Engine Technology (SET) - Task 23. ANOPP Noise Prediction for Small Engines. Wing Reflection Code // NASA/CR-2000-210630, AlliedSignal Engines and Systems, Phoenix, Arizona, 2000.